A Parametric Compact Thermal Modeling Framework for Rapid Design Space Exploration of Radial Multistage Thermoelectric Coolers

U G Nuwantha Kumara
Department of Mechanical Engineering
University of Moratuwa
Moratuwa, Sri Lanka
nuwanthakumara999@gmail.com

***Abstract*—This paper presents a Compact Thermal Model (CTM) for a multistage thermoelectric cooler (TEC) under the assumption of 1D heat transfer in thermally isolated wedges. The geometric parameters are used to form a linear system of equations representing an equivalent thermal resistance network, which can be solved to obtain temperatures at defined nodes. The CTM was verified against high-fidelity COMSOL Multiphysics simulations, demonstrating a relative error of less than 5% within a central diagonal region of the heat flux and thickness design space. While larger errors were observed at extreme combinations of some parameters, the CTM maintained exceptional trend fidelity across the majority of the design space, with Spearman rank correlation coefficients (rho) exceeding 0.93 (p less than 0.001). These results confirm that the CTM accurately preserves the global topology of the design space, making it a statistically significant tool for rapid optimization.**

***Index Terms*—thermoelectric cooling, compact thermal model, radial architecture, thermal resistance network, multi-fidelity optimization.**

I. Introduction

Heat dissipation of microelectromechanical systems (MEMS) is achieved through passive cooling at low power levels. However, active cooling becomes a necessity when power usage increases. At the microscale, traditional active cooling methods become difficult to implement [1]. Coolers utilizing the thermoelectric effect offer easier miniaturization due to their solid-state nature.

A. Thermoelectric Effect

When a current flows through a junction of two dissimilar semiconductors, the Peltier (Thermoelectric) effect causes heat to be absorbed or released at the junction due to the difference in charge-carrier energy levels. When arranged appropriately, it forms a solid-state device capable of pumping heat from one end to another. The governing equation for a thermoelectric (TE) junction is given by

$$Q_c = SIT_c - K(T_h - T_c) - \frac{1}{2}I^2R \tag{1}$$

Here, Q_c denotes the heat absorbed at the cold side of the junction. The three terms represent the Peltier effect, thermal conduction, and Joule heating, respectively. S is the Seebeck coefficient of the material that governs the TE effect while K and R represent the thermal conductivity and electrical resistance. I is the current applied through them, while T_c and T_h are the temperatures of the hot and cold sides of TEC. In this work, the cold side (Q_c) extracts heat and the hot side rejects heat, defining them by operation rather than absolute temperature.

B. Related Work

Microscale thermoelectric devices are used for many purposes such as heating, cooling, and power generation. At this scale, thermoelectric coolers (TECs) are mostly designed as layers, and two primary design architectures exist: those that transfer heat normal to the TEC layer and those that transfer heat through the thickness of the layer [2]. Radial TECs belong to the latter category and incorporate a modular and asymmetric design.

In multi-stage TEC devices, each subsequent stage must have a larger heat capacity to pump both the absorbed heat and the heat generated by preceding stages. Increasing the heat pumping capacity of subsequent stages usually requires a larger surface area, creating a conventional pyramid-like structure [3]. Conversely, a radial layout naturally expands this cross-sectional area as stages move outward. This paper develops a mathematical model to calculate junction temperatures for multi-stage radial TECs, drawing inspiration from thin-film TEC modeling in [3].

II. Methodology: Geometry

A. Geometry and Parameterization

The TEC is configured such that a single stage occupies a concentric ring, with multiple stages stacked radially outward (Fig. 1a). The TEC is located on top of the surface being cooled, and between this layer and the TEC layer, an insulation layer is required to electrically isolate the TECs (Fig. 1c). To provide a low-resistance path for heat to reach the TECs, a cylinder is placed in the center (Fig. 1g). TEC elements are sandwiched between insulators in both radial and azimuthal directions to keep the TE legs isolated, as shown in Fig. 1f. Radial insulators are concentric rings of constant width while azimuthal insulators expand radially as shown in Fig. 1e.

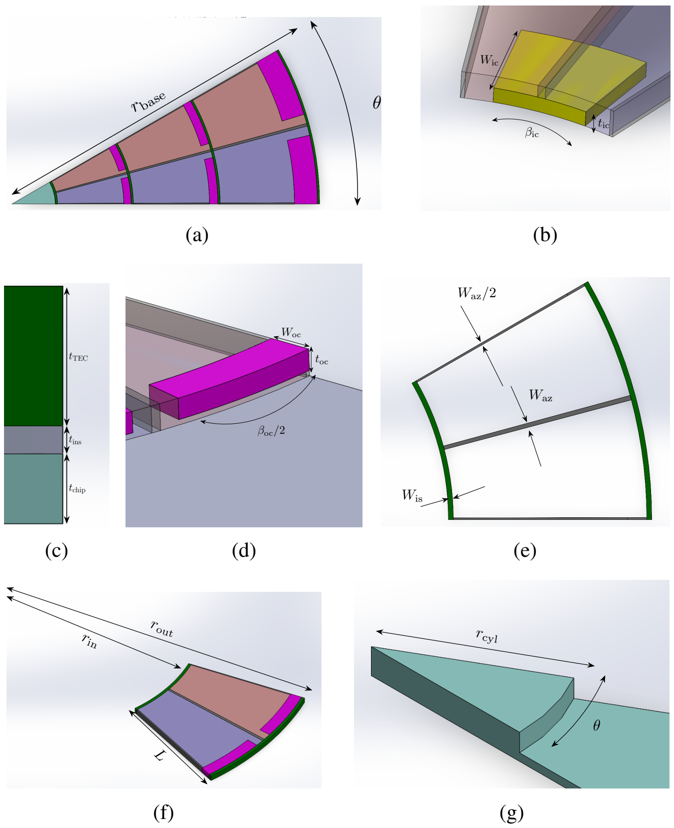

Fig. 1. Geometric annotation figures for the radial TEC model: (a) wedge top view, (b) interconnect (IC), (c) layers side view, (d) outerconnect (OC), (e) azimuthal and radial insulators top view, (f) TEC element isometric view, and (g) central cylinder. Distinct colors denote distinct material regions.

Inside a TEC element, there is a copper interconnect (IC) shown in Fig. 1b that connects the p- and n-type TE legs together. At the other end, a copper connector termed the "outerconnect" (OC) joins the consecutive p- and n-type legs between wedges, as shown in Fig. 1d, thereby simplifying the wiring. All geometric parameters are listed in Table I, while Table II lists the constraints they are subject to.

B. Dimensional Reduction

There are nine independent parameters per stage, resulting in a problem complexity of $O(9M)$. This leads to the "curse of dimensionality," making the solution space sparse at higher dimensions. Therefore, we perform a dimensional reduction by turning several parameters into ratios that depend on other parameters, and fix these ratios across all stages. The ratio parameters, which would be the independent variables of the optimization problem are listed in Table III alongside their definitions. Table IV shows how to recover geometric parameters from optimization variables. W_{is} is fixed across all stages and remains independent; thus, it is not reduced to a fractional variable. $W_{\text{az},i}$ expands radially and is not constant across stages. Therefore, f_{f} acts as an angular quantity, expressed in terms of arc length, conveying the fraction of the total radial area occupied by TE materials.

TABLE I
GEOMETRIC PARAMETERS

Symbol	Component / Description	Figure
	Thicknesses (μm)	
t_{TEC}	TEC layer	1c
t_{ins}	Electrical insulation (TEC to generation layer)	1c
t_{gen}	Heat generation layer	1c
$t_{\text{ic},i}$	Copper interconnect	1b
$t_{\text{oc},i}$	Copper outerconnect	1d
	Radii (μm)	
r_{base}	Entire TEC array base	1a
r_{cyl}	Central cylinder	1g
$r_{\text{in},i}$	TEC element inner (excluding radial insulator)	1f
$r_{\text{out},i}$	TEC element outer (excluding radial insulator)	1f
	Widths & Lengths (Radial Spans) (μm)	
L_i	TEC element length	1f
$W_{\text{is},i}$	Radial insulator	1e
$W_{\text{az},i}$	Azimuthal insulator (linear dimensions)	1e
$W_{\text{ic},i}$	Copper interconnect	1b
$W_{\text{oc},i}$	Copper outerconnect	1d
	Angles & Azimuthal Spans (rad)	
θ	Single wedge	1a
$\beta_{\text{ic},i}$	Copper interconnect	1b
$\beta_{\text{oc},i}$	Copper outerconnect	1d
	System Parameters	
M	Total number of stages ($\mathbb{N}^+$)	1a

III. Methodology: Resistance Calculations

A. Resistor Arrangement

Thermal resistances of components depend on the heat transfer direction, which is assumed purely radial, with no azimuthal or vertical heat transfer occurring within the layers. Individual resistances of all conductors must be lumped together to be used as the conduction term in the governing equation. To model this mathematically, we select nodes that connect these resistances, setting the temperatures at these nodes as the unknowns of the system.

In this formulation, the boundaries between the azimuthal and radial insulators serve as the representative nodes. Consequently, the thermal resistances between these repeating interfaces are lumped into a single resistor based on the connectivity shown in Fig. 2. As illustrated in Fig. 3, the nodes in the generation layer are vertically aligned with those in the TEC layer; thus, interlayer heat conduction is modeled via discrete thermal resistances connected between the top and bottom nodes.

B. Thermal Resistances

For a material with thermal conductivity κ and a variable cross-sectional area, the thermal resistance is defined as,

$$R_{\text{t}} = \int_{x=0}^{L} \frac{dx}{\kappa \cdot A(x)} \tag{2}$$

Most subsequent resistance formulations in this work reduce to the following standard integral:

$$\int_{x_1}^{x_2} \frac{1}{ax} dx = \frac{1}{a} \ln \left| \frac{x_2}{x_1} \right| \tag{3}$$

When calculating the thermal conductivity of the TE legs, we must divide the region radially into three separate parts

TABLE II
GEOMETRIC CONSTRAINTS

Reason	Formula
Avoiding interconnect - outerconnect contact	$W_{\text{ic},i} + W_{\text{oc},i} < L_i$
Radial span of all stages adding up to base radius	$r_{\text{base}} = r_{\text{cyl}} + \sum_{i=1}^{M} (L_i + W_{\text{is},i}) + W_{\text{is},M+1}$
Azimuthal insulator must fit inside the element	$2W_{\text{az},i} < r_{\text{in},i}\theta$
Central cylinder must be contained in the TEC	$0 < r_{\text{cyl}} < r_{\text{base}}$

TABLE III
REDUCED PARAMETER DEFINITIONS

Symbol	Name	Definition	Replaces	Bounds
N	No. of wedges	$N = 2\pi/\theta$	θ	$(2, +\infty)$
f_L	Length ratio	$f_L = L_{i+1}/L_i$	L	$(0, +\infty)$
$f_{\text{ic,w}}$	IC width frac.	$f_{\text{ic,w}} = W_{\text{ic}}/L_i$	W_{ic}	$(0, 0.5)$
$f_{\text{ic,t}}$	IC thickness frac.	$f_{\text{ic,t}} = t_{\text{ic}}/t_{\text{TEC}}$	t_{ic}	$(0, 1)$
$f_{\text{ic},\beta}$	IC angle frac.	$f_{\text{ic},\beta} = \beta_{\text{ic}}/\theta$	β_{ic}	$(0, 1)$
$f_{\text{oc,w}}$	OC width frac.	$f_{\text{oc,w}} = W_{\text{oc}}/L_i$	W_{oc}	$(0, 0.5)$
$f_{\text{oc,t}}$	OC thickness frac.	$f_{\text{oc,t}} = t_{\text{oc}}/t_{\text{TEC}}$	t_{oc}	$(0, 1)$
$f_{\text{oc},\beta}$	OC angle frac.	$f_{\text{oc},\beta} = \beta_{\text{oc}}/\theta$	β_{oc}	$(0, 1)$
f_{f}	Fill Factor	$f_{\text{f}} = 1 - \frac{W_{\text{az}}}{(\text{Arc Length})}$	W_{az}	$(0, 1)$

TABLE IV
RECOVERY MAP

Original Parameter	Recovery Formula	Notes
θ	$2\pi/N$	—
$r_{\text{in},i}$	$r_{\text{cyl}} + i \cdot W_{\text{is}} + \sum_{j=1}^{i-1} L_j$	$r_{\text{in},1} = r_{\text{cyl}} + W_{\text{is}}$
$r_{\text{out},i}$	$r_{\text{in},i} + L_i$	—
L_i	$L_1 \cdot f_L^{(i-1)}$	$L_1 = \frac{r_{\text{base}} - r_{\text{cyl}} - (M+1)W_{\text{is}}}{(1-f_L^M)/(1-f_L)}$
$W_{\text{az}}(r)$	$(1 - f_f) \cdot r\theta$	Continuous radial func.
$W_{\text{ic},i}$	$f_{\text{ic,w}} \cdot L_i$	—
$t_{\text{ic},i}$	$f_{\text{ic,t}} \cdot t_{\text{TEC}}$	—
$\beta_{\text{ic},i}$	$f_{\text{ic},\beta} \cdot \theta$	Stage-independent
$W_{\text{oc},i}$	$f_{\text{oc,w}} \cdot L_i$	—
$t_{\text{oc},i}$	$f_{\text{oc,t}} \cdot t_{\text{TEC}}$	—
$\beta_{\text{oc},i}$	$f_{\text{oc},\beta} \cdot \theta$	Stage-independent

because cross-sectional area in the first and last regions is reduced due to electrical connections:

- Region I containing interconnect: $r \in (r_{\text{in}}, r_{\text{in}} + W_{\text{ic}})$
- Region II without any connections: $(r_{\text{in}} + W_{\text{ic}}, r_{\text{out}} - W_{\text{oc}})$
- Region III containing outerconnect: $(r_{\text{out}} - W_{\text{oc}}, r_{\text{out}})$

Table V summarizes all TEC layer calculations. Heat transfer between nodes in the two layers is modeled as if heat passes through a resistance equivalent to the area occupied by half of each stage connected to the node. Thus, for the i^{th} node, the area lies within the radial span $(r_{\text{in},i} - L_{i-1}/2, r_{\text{in},i} + L_i/2)$ which can be calculated using $\frac{\theta}{2}(r_2^2 - r_1^2)$, resulting

$$R_{\text{ve},i} = \frac{2t_{\text{ins}}}{\kappa_{\text{ins}}\theta}\left[\left(r_{\text{in},i} - \frac{L_{i-1}}{2}\right)^2 - \left(r_{\text{in},i} + \frac{L_i}{2}\right)^2\right]^{-1} \tag{4}$$

The central cylinder can be denoted as Node 0, a node common to both layers (Fig. 1g). Hence, the resistance between Node 0 and Node 1 of both layers is needed. The standard formula (2) with limit $r = 0$ at the cylinder's center fails due to the singularity. Approximating via the solution for volumetric cylinder generation, $T_{\text{center}} - T_{\text{surf}} = \frac{Q}{4\pi k t}$, and scaling for a wedge angle θ (replacing 4π with 2θ), the center-to-surface thermal resistance is:

$$R_{\text{cyl}} = \frac{1}{2\theta\kappa t} \tag{5}$$

While $R_{\text{gen},0\to1}$ for the generation layer follows directly from the equation above, the TEC layer requires adding the resistance of the first radial insulator in series, as it precedes the first TEC element.

$$R_{\text{TEC},0\to1} = \frac{1}{2\theta\kappa_{\text{gen}}t_{\text{TEC}}} + R_{\text{is},0} \tag{6}$$

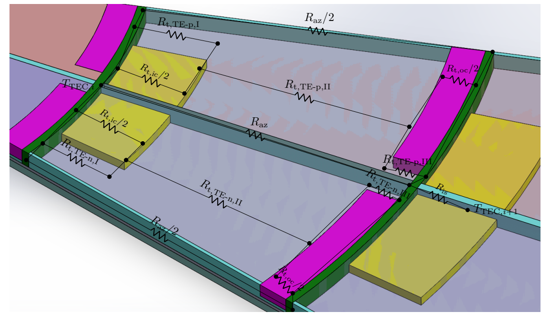

Fig. 2. Thermal resistor arrangement within a TEC element.

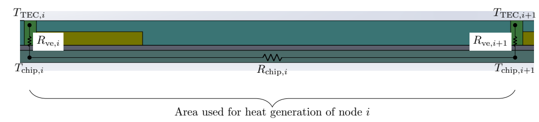

Fig. 3. Side-view resistor arrangement including chip layer and vertical coupling.

C. Electrical Resistances

The electrical resistance for a variable cross-sectional area with resistivity ρ is given by:

$$R_{\text{e}} = \int_{x=0}^{L} \frac{\rho \cdot dx}{A(x)} \tag{7}$$

For the TE leg, we omit regions I and III for heat generation, which is justified since region II bridges the IC and OC electrical path, and current naturally follows the path of least resistance. After solving the integral, we get

$$R_{\text{e,TE,II}} = \frac{2\rho_{\text{TE}}}{\theta \cdot t_{\text{TEC}}(2f_f - 1)} \ln\left(\frac{r_{\text{out}} - W_{\text{oc}}}{r_{\text{in}} + W_{\text{ic}}}\right) \tag{8}$$

The electrical connections transfer electricity mainly in the azimuthal direction; thus, the infinitesimal strips are in parallel, and the integration must be performed over the conductance.

$$G_{\text{total}} = \int_{r_1}^{r_2} \frac{t_{\text{ic}}}{\rho_{\text{TE}}\beta_{\text{ic}}}\frac{1}{r}dr = \frac{t_{\text{ic}}}{\rho_{\text{TE}}\beta_{\text{ic}}} \ln\left(\frac{r_2}{r_1}\right) \tag{9}$$

Therefore, the resistances are,

$$R_{\text{e,ic}} = \frac{\rho_{\text{TE}}\beta_{\text{ic}}}{t_{\text{ic}} \ln\left(\frac{r_{\text{in}} + W_{\text{ic}}}{r_{\text{in}}}\right)} \tag{10}$$

$$R_{\text{e,oc}} = \frac{\rho_{\text{TE}}\beta_{\text{oc}}}{t_{\text{oc}} \ln\left(\frac{r_{\text{out}}}{r_{\text{out}} - W_{\text{oc}}}\right)} \tag{11}$$

TABLE V
THERMAL RESISTANCE EXPRESSIONS

Component	Area	Limits	Final Expression (Original)	Reduced Expression (Optimization Variables)
TE Leg I ($R_{\text{t,TE,I}}$)	$\frac{r}{2}\left[\theta \cdot t_{\text{TEC}}(2f_f-1) - \beta_{\text{ic}} \cdot t_{\text{ic}}\right]$	$(r_{\text{in}}, r_{\text{in}} + W_{\text{ic}})$	$\frac{2}{\kappa_{\text{TE}}[\theta t_{\text{TEC}}(2f_f-1)-\beta_{\text{ic}} t_{\text{ic}}]} \ln\left(\frac{r_{\text{in}}+W_{\text{ic}}}{r_{\text{in}}}\right)$	$\frac{N}{\pi\kappa_{\text{TE}} t_{\text{TEC}}[2f_f-1-f_{\text{ic},\beta} f_{\text{ic,t}}]} \ln\left(1 + f_{\text{ic,w}} \frac{L_i}{r_{\text{in},i}}\right)$
TE Leg II ($R_{\text{t,TE,II}}$)	$\frac{1}{2} r\theta \cdot t_{\text{TEC}}(2f_f-1)$	$(r_{\text{in}} + W_{\text{ic}}, r_{\text{out}} - W_{\text{oc}})$	$\frac{2}{\kappa_{\text{TE}}\theta \cdot t_{\text{TEC}}(2f_f-1)} \ln\left(\frac{r_{\text{out}}-W_{\text{oc}}}{r_{\text{in}}+W_{\text{ic}}}\right)$	$\frac{N}{\pi\kappa_{\text{TE}} t_{\text{TEC}}(2f_f-1)} \ln\left(\frac{r_{\text{in},i}+L_i(1-f_{\text{oc,w}})}{r_{\text{in},i}+f_{\text{ic,w}} L_i}\right)$
TE Leg III ($R_{\text{t,TE,III}}$)	$\frac{r}{2}\left[\theta \cdot t_{\text{TEC}}(2f_f-1) - \beta_{\text{oc}} \cdot t_{\text{oc}}\right]$	$(r_{\text{out}} - W_{\text{oc}}, r_{\text{out}})$	$\frac{2}{\kappa_{\text{TE}}[\theta t_{\text{TEC}}(2f_f-1)-\beta_{\text{oc}} t_{\text{oc}}]} \ln\left(\frac{r_{\text{out}}}{r_{\text{out}}-W_{\text{oc}}}\right)$	$\frac{N}{\pi\kappa_{\text{TE}} t_{\text{TEC}}[2f_f-1-f_{\text{oc},\beta} f_{\text{oc,t}}]} \ln\left(\frac{r_{\text{in},i}+L_i}{r_{\text{in},i}+L_i(1-f_{\text{oc,w}})}\right)$
Interconnect ($R_{\text{t,ic}}$)	$r \cdot \beta_{\text{ic}} \cdot t_{\text{ic}}$	$(r_{\text{in}}, r_{\text{in}} + W_{\text{ic}})$	$\frac{1}{\kappa_{\text{TE}} \cdot \beta_{\text{ic}} \cdot t_{\text{ic}}} \ln\left(\frac{r_{\text{in}}+W_{\text{ic}}}{r_{\text{in}}}\right)$	$\frac{N}{2\pi\kappa_{\text{TE}} f_{\text{ic},\beta} f_{\text{ic,t}} t_{\text{TEC}}} \ln\left(1 + f_{\text{ic,w}} \frac{L_i}{r_{\text{in},i}}\right)$
Outerconnect ($R_{\text{t,oc}}$)	$r \cdot \beta_{\text{oc}} \cdot t_{\text{oc}}$	$(r_{\text{out}} - W_{\text{oc}}, r_{\text{out}})$	$\frac{1}{\kappa_{\text{TE}} \cdot \beta_{\text{oc}} \cdot t_{\text{oc}}} \ln\left(\frac{r_{\text{out}}}{r_{\text{out}}-W_{\text{oc}}}\right)$	$\frac{N}{2\pi\kappa_{\text{TE}} f_{\text{oc},\beta} f_{\text{oc,t}} t_{\text{TEC}}} \ln\left(\frac{r_{\text{in},i}+L_i}{r_{\text{in},i}+L_i(1-f_{\text{oc,w}})}\right)$
Radial Insulator ($R_{\text{t,is}}$)	$r \cdot \theta \cdot t_{\text{TEC}}$	$r_{\text{out}} \to r_{\text{out}} + W_{\text{is}}$	$\frac{1}{\kappa_{\text{is}} \cdot \theta \cdot t_{\text{TEC}}} \ln\left(\frac{r_{\text{out}}+W_{\text{is}}}{r_{\text{out}}}\right)$	$\frac{N}{2\pi\kappa_{\text{is}} t_{\text{TEC}}} \ln\left(1 + \frac{W_{\text{is}}}{r_{\text{in},i}+L_i}\right)$
Azimuthal Insulator (R_{az})	$(1-f_f)\theta \cdot t_{\text{TEC}} \cdot r$	$(r_{\text{in}}, r_{\text{out}})$	$\frac{1}{\kappa_{\text{az}}(1-f_f)\theta \cdot t_{\text{TEC}}} \ln\left(\frac{r_{\text{out}}}{r_{\text{in}}}\right)$	$\frac{N}{2\pi\kappa_{\text{az}}(1-f_f) t_{\text{TEC}}} \ln\left(1 + \frac{L_i}{r_{\text{in},i}}\right)$
Chip layer (R_{gen})	$r \cdot \theta \cdot t_{\text{gen}}$	$(r_{\text{in}}, r_{\text{out}})$	$\frac{1}{\kappa_{\text{gen}} \cdot \theta \cdot t_{\text{gen}}} \ln\left(\frac{r_{\text{out}}}{r_{\text{in}}}\right)$	$\frac{N}{2\pi\kappa_{\text{gen}} t_{\text{gen}}} \ln\left(1 + \frac{L_i}{r_{\text{in},i}}\right)$

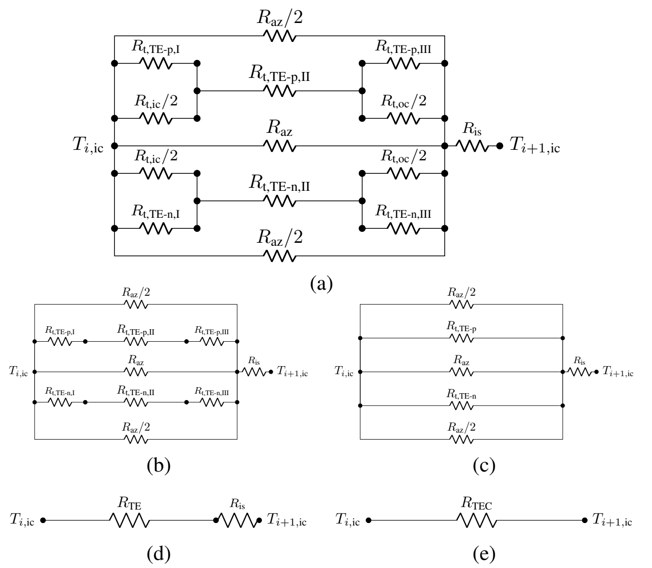

Fig. 4. Step-by-step compaction of the thermal resistor network of a single TEC element. (a) Original arrangement. (b) Parallel resistors in regions I and III are absorbed into $R_{\text{t,TE-p,I/III}}$ and $R_{\text{t,TE-n,I/III}}$. (c) Series combination yields the total leg resistances $R_{\text{t,TE-p}}$ and $R_{\text{t,TE-n}}$. (d) The five parallel branches collapse into R_{TE}. (e) Series combination with the radial insulator gives R_{TEC}.

D. Lumping Resistances

The complete resistor arrangement from Fig. 2 is presented in a simplified schematic in Fig. 4a. The corresponding circuit reductions from step (b) through step (e) are evaluated sequentially using (12a)–(12d):

$$\frac{1}{R_{\text{t,TE-p,I,new}}} = \frac{1}{R_{\text{t,TE-p,I}}} + \frac{2}{R_{\text{t,ic}}} \tag{12a}$$

$$R_{\text{t,TE-p}} = R_{\text{t,TE-p,I,new}} + R_{\text{t,TE-p,II}} + R_{\text{t,TE-p,III}} \tag{12b}$$

$$\frac{1}{R_{\text{TE}}} = \frac{2}{R_{\text{az}}} + \frac{1}{R_{\text{t,TE-p}}} + \frac{1}{R_{\text{t,TE-n}}} \tag{12c}$$

$$R_{\text{TEC}} = R_{\text{TE}} + R_{\text{is}} \tag{12d}$$

IV. FORMATION OF THE LINEAR SYSTEM

To find the temperature values at each node, we can set up a system of linear equations by writing energy balance equations for the three available types of nodes: generation layer nodes, TEC layer nodes, and the central node.

A. Generation Layer

A general node in this layer comprises four terms: two for lateral heat transfer, one for vertical heat transfer to the TEC layer, and one for heat generation from the applied heat flux. The energy balance equation is given by:

$$\underbrace{\frac{T_{\text{gen},i-1} - T_{\text{gen},i}}{R_{\text{gen},i-1}}}_{\text{Lateral In}} + \underbrace{\frac{T_{\text{gen},i+1} - T_{\text{gen},i}}{R_{\text{gen},i}}}_{\text{Lateral Out}} - \underbrace{\frac{T_{\text{gen},i} - T_{\text{TEC},i}}{R_{\text{ve},i}}}_{\text{Vertical Loss}} + Q_{\text{gen},i} = 0 \tag{13}$$

Due to its closed topology, this layer lacks boundary conditions. However, when formulating the equation for the first node, the term $R_{\text{gen},i-1} = R_{\text{gen},0}$ is replaced by $R_{\text{gen},0\to 1}$, given by (5).

B. TEC Layer

Substituting the reciprocals of the derived resistances into (1) and applying the localized Joule heating allocations from Table VI, the energy balance for a TEC layer node yields:

$$\underbrace{\frac{T_{\text{gen},i} - T_{c,i}}{R_{\text{ve},i}}}_{\text{From gen. layer}} + \underbrace{Q_{h,i-1}}_{\text{From Stage } i-1} - \underbrace{Q_{c,i}}_{\text{Into Stage } i} = 0 \tag{14}$$

where,

$$\begin{aligned} Q_{h,i-1} &= S_{i-1} I_{i-1} T_{\text{TEC},i-1} - K_{t,i-1}(T_{\text{TEC},i} - T_{\text{TEC},i-1}) \\ &\quad + \underbrace{\left[\frac{1}{2} I_{i-1}^2 (R_{\text{TE-p},i-1} + R_{\text{TE-n},i-1}) + I_{i-1}^2 R_{e,\text{oc},i-1}\right]}_{\text{Joule Heat at Hot Side}} \\ Q_{c,i} &= S_i I_i T_{c,i} - K_{t,i}(T_{\text{TEC},i+1} - T_{\text{TEC},i}) \\ &\quad - \underbrace{\left[\frac{1}{2} I_i^2 (R_{\text{TE-p},i} + R_{\text{TE-n},i}) + I_i^2 R_{e,\text{ic},i}\right]}_{\text{Joule Heat at Cold Side}} \end{aligned} \tag{15}$$

The Joule heating term carries a negative sign within the subtracted cooling term (Q_c) to correctly represent a net heat addition to the local node. As with the chip layer, the first-node substitution requires setting $K_{\text{t},i-1} = K_{\text{t},0} = 1/R_{\text{TEC},0\to 1}$ per (6). The conductances K_{t} are obtained from the lumped thermal resistances in (12d). For the final TEC node, applying

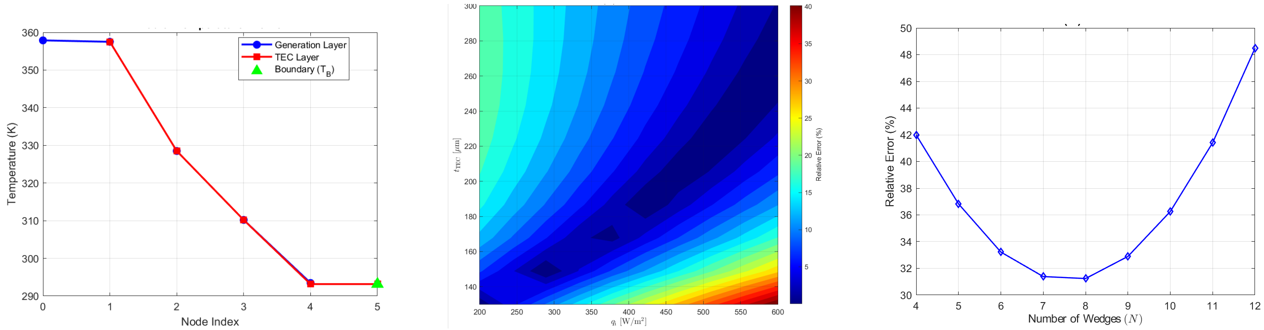

(a) (b) (c)

Fig. 5. Thermal and parametric error analysis: (a) Nodal temperature plot, (b) 2-D parametric sweep of relative error, and (c) relative error variation with wedge count.

TABLE VI
HEAT CONTRIBUTION BREAKDOWN FOR NODE $T_{c,i}$

Component(s)	**Heat Contribution**
IC of Stage i	$100\% \times I_i^2 R_{e,ic,i}$
Legs of Stage i	$50\% \times (I_i^2 R_{e,TE-p,i} + I_i^2 R_{e,TE-n,i})$
OC of Stage $(i-1)$	$100\% \times I_{i-1}^2 R_{e,oc,i-1}$
Legs of Stage $(i-1)$	$50\% \times (I_{i-1}^2 R_{e,TE-p,i-1} + I_{i-1}^2 R_{e,TE-n,i-1})$

a constant temperature boundary condition ($T_{\text{TEC},n+1} = T_{\text{B}}$) shifts this known term to the right-hand side of the equation.

C. Central Node and Matrix Assembly

Denoting the central node temperature as T_0, we can write the energy balance equation for this central node as:

$$\frac{T_{\text{gen},1} - T_0}{R_{\text{gen},0\to1}} + \frac{T_{\text{TEC},1} - T_0}{R_{\text{TEC},0\to1}} - Q_{\text{gen},0} = 0$$

The energy balance equations yield the linear system $\mathbf{A} \cdot \mathbf{T} = \mathbf{B}$, where $\mathbf{A}$ is the coefficient matrix containing lumped thermal resistances, $\mathbf{T}$ is the unknown nodal temperature vector, and $\mathbf{B}$ contains heat generation and boundary conditions. In partitioned block form, this system is structured as:

$$\begin{bmatrix} \mathbf{A_{00}} & \mathbf{L}_{0\to\text{Si}} & \mathbf{L}_{0\to\text{TEC}} \\ \mathbf{L}_{\text{Si}\to0} & \mathbf{A_{gen}} & \mathbf{A_{ve}} \\ \mathbf{L}_{\text{TEC}\to0} & \mathbf{A_{ve}} & \mathbf{A_{TEC}} \end{bmatrix} \begin{bmatrix} T_0 \\ \mathbf{T}_{\text{gen}} \\ \mathbf{T}_{\text{TEC}} \end{bmatrix} = \begin{bmatrix} \mathbf{B_0} \\ \mathbf{B}_{\text{gen}} \\ \mathbf{B}_{\text{TEC}} \end{bmatrix} \quad (16)$$

Once solved, derived performance metrics such as total electrical power input and coefficient of performance (COP) are directly recoverable from the nodal temperatures and electrical resistances.

V. RESULTS AND VALIDATION

A. Validation Setup

To validate the CTM, a MATLAB implementation was compared against high-fidelity COMSOL Multiphysics simulations. The geometry was managed via a parameterized SolidWorks model connected through LiveLink, with COMSOL's MATLAB API automating the parametric sweeps.

The base case parameters are detailed in Table VII. The model utilizes Bi_2Te_3 as the thermoelectric material, Cu for

TABLE VII
BASE CASE PARAMETERS

Parameter	**Value**	**Parameter**	**Value**
N	12	$f_{\text{ic,w}}$	0.1
M	3	$f_{\text{ic,t}}$	0.6
r_{base}	10000 μm	$f_{\text{ic},\beta}$	0.5
t_{gen}	50 μm	$f_{\text{oc,w}}$	0.1
t_{TEC}	150 μm	$f_{\text{oc,t}}$	0.6
t_{ins}	20 μm	$f_{\text{oc},\beta}$	0.5
r_{cyl}	1000 μm	f_{f}	0.9
f_{L}	1.15		

electrical interconnects, and SiO_2 and Al_2O_3 as insulators. For subsequent analyses, the maximum temperature serves as the primary performance metric, and the relative error is evaluated with respect to the cold reservoir boundary temperature (293.15 K or 20°C).

The nodal temperature profile computed by the CTM is illustrated in Fig. 5a. The temperature gradient between layers is minimal due to the low thermal resistance afforded by the high surface-area-to-thickness ratio. Furthermore, the first two nodes exhibit identical temperatures owing to the low inter-nodal thermal resistance driven by the relatively high thermal conductivity of the silicon cylinder ($150\ \text{W}/(\text{m}\cdot\text{K})$). Computationally, a single CTM evaluation completes in approximately 83 ms in MATLAB, compared to approximately 2.2 minutes per COMSOL simulation, yielding a speedup of roughly 1570x.

B. Valid Domain

Given that TEC thickness and heat load are the primary design drivers, a 2D parametric sweep was conducted (Fig. 5b). A distinct diagonal band exhibits minimal error ($< 5\%$), with discrepancies increasing progressively as the parameter combinations deviate from this region. This divergence is hypothesized to stem from localized nonlinear behaviors unaccounted for in the 1D framework.

The relative error variation with the wedge count N exhibits a characteristic parabolic trend with a distinct minimum (Fig. 5c), driven by competing geometric regimes. Small values of N yield wide wedge angles that disrupt the 1D

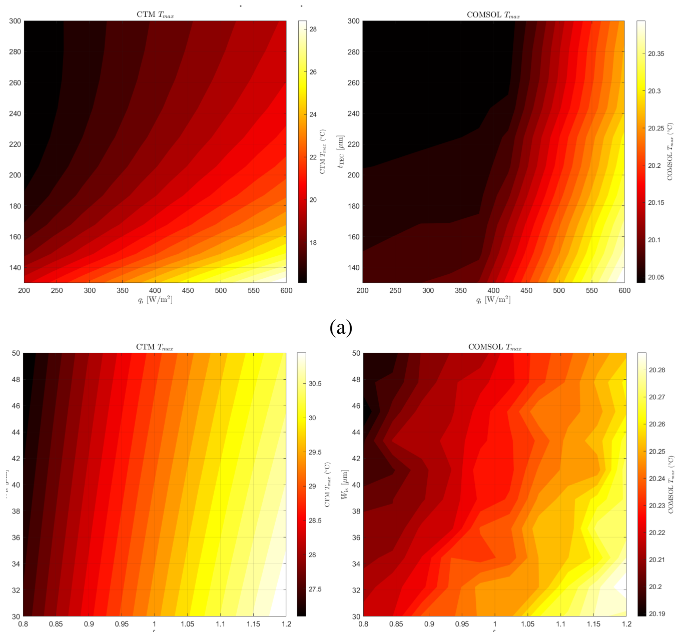

Fig. 6. 2D parametric sweeps comparison: (a) q vs t_{TEC}, (b) f_L vs $W_{\text{is},i}$

radial flow approximation. Modest increases in N narrow the domain, properly enforcing radial conduction. Conversely, an excessive wedge count sharply reduces the azimuthal insulator width (W_{az}), permitting cross-wedge azimuthal heat transfer that violates the radial flow assumption.

C. Trend Fidelity Analysis

Although 1D simplifying assumptions can introduce relative errors, deploying the CTM as a design optimization tool primarily requires the model to accurately capture high-fidelity design space trends. To quantify this alignment, Kendall's Tau-b (τ_b) and Spearman's rank correlation coefficient (ρ) were evaluated [4]–[6].

The statistical outcomes from several 2D parametric sweeps, computed via the MATLAB `corr` function [7], are summarized in Table VIII. The CTM demonstrates exceptional trend fidelity ($\rho > 0.93$) across the majority of the design space. Highly significant p-values ($p < 0.001$) confirm that the CTM preserves the global trend structure, validating its suitability for optimization tasks. This tracking behavior is visually confirmed by the side-by-side contours in Fig. 6, where the CTM temperature variations closely mirror the COMSOL profiles while exhibiting inherently smoother distributions due to their underlying analytical formulation.

Discrepancies in this trend alignment primarily arise when evaluating parameters that govern the insulation geometry, such as f_{f} and $W_{\text{is},i}$. This degradation occurs at the extreme bounds of the parametric sweep, which induce highly disproportionate TEC geometries. For instance, an excessively large fill factor (f_{f}) results in ultra-thin insulation layers that facilitate parasitic azimuthal heat transfer.

TABLE VIII
RANK CORRELATION SUMMARY OF DESIGN SPACE SWEEPS

	Spearman (ρ)		Kendall (τ)	
Sweep Parameters	**Value**	**p-value**	**Value**	**p-value**
f_L vs $W_{\text{is},i}$	0.9634		0.8440	
f_L vs t_{TEC}	0.9496		0.8174	
f_L vs q	0.9459		0.8242	
$W_{\text{is},i}$ vs t_{TEC}	0.9907	< 0.001	0.9301	< 0.001
$W_{\text{is},i}$ vs q	0.9375		0.8275	
f_f vs t_{TEC}	0.9284		0.7507	
q vs t_{TEC}	0.8281		0.6505	
f_f vs q	0.8163		0.6109	
f_L vs f_f	0.1804	0.0724	0.1261	0.0635
f_f vs $W_{\text{is},i}$	-0.1387	0.1688	-0.0784	0.2491

VI. LIMITATIONS AND FUTURE WORK

The 1D radial heat flow assumption limits model accuracy to moderate geometric configurations; at extreme parameter combinations, multi-dimensional thermal effects introduce larger deviations.

The proposed radial multistage architecture is novel, and no published experimental benchmarks exist; fabrication facilities were also unavailable for this study. Experimental characterization, formal optimization studies, and global sensitivity analysis leveraging the CTM's computational efficiency are identified as natural extensions of this framework.

VII. CONCLUSION

This paper presents a Compact Thermal Model (CTM) for radial multistage thermoelectric coolers (TECs) based on a 1D thermal resistance network. By modeling the device as a series of thermally isolated wedges, the framework allows for the rapid generation of nodal temperature profiles, bypassing the computational intensity of traditional FEA methods. The model shows high accuracy within nominal parameter combinations, while statistical evaluation using Kendall's Tau-b and Spearman's rank correlation confirms that the CTM mirrors high-fidelity results with a correlation above 0.93. This ensures that the design space topology is preserved, allowing the model to be used reliably for optimization, even in regions with higher relative error.

REFERENCES

[1] C. Li, Y. Luo, W. Li, B. Yang, C. Sun, W. Ma, Z. Ma, Y. Wei, X. Li, and J. Yang, "The on-chip thermoelectric cooler: Advances, applications and challenges," *Chip*, vol. 3, no. 2, p. 100096, Jun. 2024.

[2] O. Owoyele, S. Ferguson, and B. T. O'Connor, "Performance analysis of a thermoelectric cooler with a corrugated architecture," *Applied Energy*, vol. 147, pp. 184–191, Jun. 2015.

[3] G. Hwang, A. Gross, H. Kim, S. Lee, N. Ghafouri, B. Huang, C. Lawrence, C. Uher, K. Najafi, and M. Kaviany, "Micro thermoelectric cooler: Planar multistage," *International Journal of Heat and Mass Transfer*, vol. 52, no. 7-8, pp. 1843–1852, Mar. 2009.

[4] C. Spearman, "The Proof and Measurement of Association between Two Things," *The American Journal of Psychology*, vol. 15, no. 1, p. 72, Jan. 1904.

[5] M. G. Kendall, "A NEW MEASURE OF RANK CORRELATION," *Biometrika*, vol. 30, no. 1-2, pp. 81–93, Jun. 1938.

[6] ——, "THE TREATMENT OF TIES IN RANKING PROBLEMS," *Biometrika*, vol. 33, no. 3, pp. 239–251, 1945.

[7] MathWorks, "Corr - linear or rank correlation - MATLAB," https://in.mathworks.com/help/stats/corr.html, accessed: Apr. 18, 2026.